Preliminary Electric Motor Drivetrain Optimization Studies for Urban Air Mobility Vehicles

Thomas Tallerico, Jeffryes Chapman, and Andrew D. Smith
NASA Glenn Research Center
thomas.tallerico@nasa.gov

***Abstract*- Electric and hybrid electric aircraft require high performance and reliable electric motor drivetrains. These drivetrains, consisting of a motor, an inverter, a gearbox, and a thermal management system, are highly coupled systems where the design of individual components in the drivetrain will significantly affect the sizing and performance of the other components in the system. In this paper, a preliminary co-optimization tool for electric motor drivetrains for Urban Air Mobility vehicles is presented. An example study with the tool is completed for NASA's RVLT quadrotor concept vehicle.**

I. INTRODUCTION

Electric and hybrid electric vertical takeoff and landing (EVTOL) vehicles require high performance and reliable electric motor drivetrains. An electric motor drivetrain consists of a motor, a motor controller/inverter, a thermal management system (TMS), and optionally a gearbox. The design of each of these components is highly coupled to the design of the other components in the drivetrain. Motor rotational speed directly affects the mass and efficiency of a gearbox. Motor inductance, power factor, modulation index, and electrical frequency affects the needed switching frequency and filter size in the inverter. Heat generated by and required coolant temperature for all components directly sizes the mass, drag, and pumping power of the TMS.

In this paper, a preliminary design tool for EVTOL motor drivetrains is presented. The goals of developing this tool are

1. To gain better understanding of the optimum design of electrical aircraft drivetrains.
2. To enable technology trade studies that quantify the full system impact of different technologies

This work builds on the EVTOL motor design tool presented in [1]. Preliminary analytical models for gearboxes, inverters, and the TMS are coupled to the motor model from [1]. Additionally, based on the results of [1], a motor stator coil mechanical stress model is incorporated into the optimizations. An example optimization with baseline technologies is completed for NASA's Revolutionary Vertical Lift Technology (RVLT) project 6 passenger all electric quadrotor concept vehicle assuming a rotor/fan speed of 1000 RPM [2].

In the following sections, first the details of the design tool are discussed in Section II. Then, the example study results are presented and discussed in Section III. Finally, a conclusion is provided summarizing the results of this preliminary optimization.

II. ELECTRIC MOTOR DRIVETRAIN DESIGN TOOL

The version of the electric motor drivetrain design tool for this paper is shown graphically in Figure 1. In the tool, a genetic optimizer is wrapped around sequential optimizations of the motor, inverter, and thermal management system. The gearbox mass and efficiency are defined by curve fits to preoptimized one and two stage gearboxes for the target power level, propellor speed, and propellor loading. The following sections provide descriptions of the variables, models, and optimization methodologies used in each box of Figure 1.

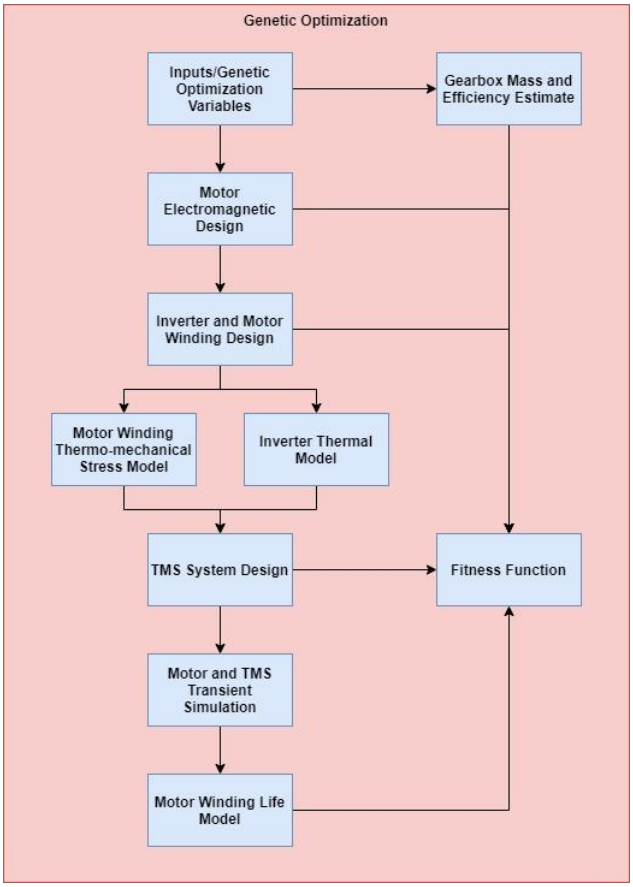

Figure 1 Design Tool Optimization Flow Diagram

A. Inputs, Assumptions, and Genetic Optimization Variables

The design tool requires inputs of component topologies, materials, and basic geometric assumptions. For the design tool runs in this paper, Table 1 summarizes the key inputs and assumptions.

Table 1Design Tool Inputs and Assumptions

Motor Assumptions and Constraints	
Motor Type	Fractional Slot PMSM
Motor Cooling	External Water Jacket
Rotor Type	In Runner Surface Mounted PM
Magnet Array	6 Magnet Halbach
Magnet Material	SmCo
Magnet Laminations	2 mm
Magnet Fill Percentage	90%
Magnet Effective Br	~1T
Stator Slot per Pole per Phase	0.5
Stator Lamination Material	0.1 mm Laminated FeCo
Insulation Thermal Class	220 C
Max Coil Shear Stress	13 MPa
Minimum Mission Efficiency	93%
Inverter Assumptions and Constraints	
Inverter Topology	2 level Voltage Source Inverter
Inverter Switch	Silicon Carbide MOSFET [3]
Allowable Switch Temperature	120 C
Max Switching Frequency	80 kHz
DC Bus Voltage	750 V
Capacitor Voltage Ripple	1% of Bus
Inductor Material	$Co_{75.4}Fe_{2.3}Mn_{2.3}Nb_4B_{14}Si_2$ [4]
Minimum Mission Efficiency	93%
Coolant Assumptions	
Thermal Conductivity	0.14 W/(m*K)
Specific Heat	2000 J/(kg*K)
Density	900 kg/m^3
Viscosity	30 cSt

The assumed mission profile for propulsion system design is the double hop mission defined in [5]. The power levels and times for the mission used in this paper are summarized in Table 2. The short down time for loading and unloading between the two flights of the mission is neglected. Collective control is assumed such that motor RPM is constant through the entire mission. Vehicle maneuvers and control responses are also neglected assuming they are short duration fluctuations around the average power level in Table 2.

Table 2 Design Mission Profile

Assumed Quadrotor Propulsion Mission Profile		
Mission Segment	**Power (kW)**	**Time (s)**
Hover1 (takeoff 1)	100	40
Climb1	140	240
Cruise1	70	1200
Hover2 (land 1 + takeoff 2)	100	80
Climb2	140	240
Cruise2	70	1200
Hover3 (land 2	100	40
Emergency	133	120

At the top level of the optimization only 6 genetic optimization variables are used. Table 3 provides the list of variables. These top level genetic optimization variables are selected to enable the sequential optimization within the tool. Motor pole count, electrical frequency, and coolant flow rate are all used at the top level because they are key drivers of the sizing of multiple components. Electrical frequency is a key driver for both motor and inverter optimization. Electrical frequency combined with machine pole count sets the rotational speed of the motor and correspondingly the required gear ratio in the gearbox. Coolant flow rate allows the motor, inverter, and TMS heat sinks and heat exchangers to be sized sequentially while maintaining compatibility with one another.

Motor mass is used as a top level variable to allow optimization of the motor for efficiency and thermal performance within the fitness function. Motor rotor tip speed and magnet thickness are used at the top level to reduce the computational complexity of the internal motor optimization. They could be integrated in at a lower level at the cost of additional computational time within each fitness evaluation.

Table 3 Genetic Optimization Variables for the Design Tool

Genetic Optimization Variables	
Motor Pole Count	Motor Electrical Frequency
Motor Tip Speed	Motor Mass
Motor Magnet Thickness	Coolant Flow Rate

B. Gearbox Mass and Efficiency

Gearbox mass and efficiency trends with gear ratio in the design tool are generated before the optimization as described in [6]. Gearboxes are designed for continuous operation at the mission's peak torque operating condition. Curve fits are applied to the optimization data and then used in the optimization to estimate gearbox efficiency and mass for a given motor RPM. For the study completed in this paper, the assumed power of the gearbox is 140 kW and the assumed output shaft speed is 1000 RPM. The resulting estimate for gearbox mass as a function of gear ratio is

$$M_{gearbox} = 14.394 * GR^{0.1493} \quad (1)$$

Gearbox efficiency is assumed to be 99.1% for a gear ratio less than 12 and 98% for a gear ratio greater than 12. This change in efficiency assumes the gearbox goes from 1 to 2 stages at a gear ratio of 12 which is potentially an overly optimistic assumption for how high a gear ratio can be achieved with a single stage.

C. Motor Electromagnetic Design

For a given set of input parameters, motor electromagnetic analysis and design is completed in 4 steps:

1. Analytical equation based optimization
2. Static FEA based optimization
3. Static FEA current and inductance calculation
4. Pseudo time stepping FEA

Inputs into the motor optimization from the genetic algorithm are the pole count, electrical frequency, motor mass, magnet thickness, and motor rotor tip speed. For the analytical optimization, motor performance is calculated for all possible combinations of predefined sets of stator thicknesses, stator tooth widths, stator back iron thicknesses, and heat sink fin heights. First for each combination the stack length of the resulting machine is calculated such that the mass is roughly equivalent to the input motor mass. Then the magnetic field produced in the airgap by the rotor Halbach arrays is calculated using the analytical equations defined in [7]. Required stator current densities and stator back iron flux densities are calculated, and loss estimates are created per the method described in [1] for every possible machine. Heat sink fin count is optimized for each design such that effective convection is maximized while keeping the flow laminar to avoid significant pumping losses. A motor geometry is selected by choosing the combination of stator iron thicknesses, stator radial thickness, and heat sink fin height that minimizes

$$\frac{Loss}{h_{conv} * A_{sink}} \quad (2)$$

Where Loss is the total power loss calculated for a machine, h_{conv} is the convection coefficient in the heat sink, and A_{sink} is the total wetted surface area in the heat sink. A thermal reluctance model is used to verify that the selected design has good thermal performance. If the selected design does not meet minimum performance requirements, the input variable set is assigned a fitness of zero.

The design from the analytical optimization is then analyzed using 2D static electromagnetic FEA. An example geometry and result for this analysis is shown in Figure 2. A stator current sweep is carried out to get field and torque data as a function of stator current. The geometry is then adjusted by repeating the optimization process used in the analytical optimization but using the FEA predicted field and torque data instead of analytical estimates.

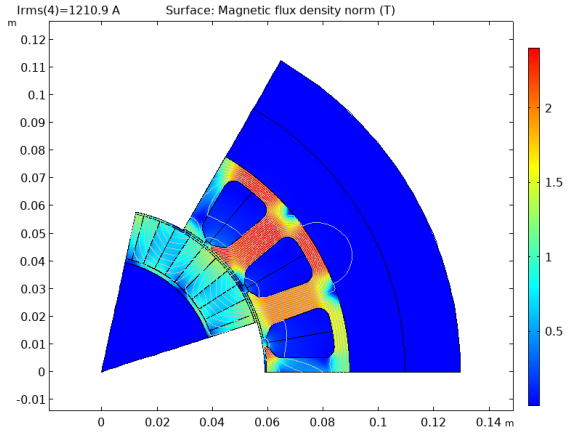

Figure 2 Example Electromagnetic FEA Geometry and Result

After the geometry adjustment with the static FEA optimization, a second static FEA simulation is performed on the adjusted geometry to calculate required current and stator single turn inductance at each mission design point. Inductance calculations are caried out using the method from [8]. Pseudo time stepping FEA analysis is then completed for the geometry and higher fidelity electromagnetic loss estimates are obtained using the method described in [1].

D. Inverter and Winding Design

Motor winding design in terms of wire gage, wires in parallel, and turns is iteratively designed with an inverter to find the minimum mass inverter that can meet the target performance requirements while minimizing combined motor winding and inverter losses. First, an inverter mass target is set to a min value. Optimum wire gage and wires in hand is then defined for all possible motor turn counts in order to minimize combined motor winding AC and DC losses in climb.

Required inverter filter sizes and inverter losses are defined for all possible motor winding turn counts, inverter switching frequencies (in 5kHz intervals), inverter inductor permeabilities, and inverter switch counts. Inverter switching losses are predicted based on [9]. The method presented in [10] is used for estimation of current ripple and all designs with too large of ripple are eliminated. Inductor mass and loss predictions are made using a basic electromagnetic circuit and geometric assumptions. DC link capacitors are sized, and loss predictions are made based on [11] [12]. As was done for the motor, heatsinks are sized to maximize cooling with laminar flow within the mass limit of the inverter for a given iteration. A basic linear thermal circuit model is used to estimate switch temperatures and eliminate designs with bad thermal performance. A design is selected to minimize combined motor winding and inverter losses in climb below the target mass value. Losses are then projected for the other flight conditions for both the inverter and the motor windings. If a design that meets minimum target performance parameters is not found, inverter design is repeated with target mass increased by 2 kg.

It should be noted that the inverter mass accounted for here only represents the main power electronics components and the heat sink. Micro controllers, cabling, and sensors are all neglected in this version of the model with the focus beginning only on the components that scale with motor characteristics and produce high losses.

E. Inverter Thermal FEA

A steady state inverter thermal model is used to define the max allowable coolant temperature the inverter can handle. An example simulation geometry and result can be seen in Figure 3. All 4 mission design points are simulated. A steady state simulation is used due to the low thermal inertia of the inverter switches and heat sink. The max temperature rise between the coolant temperature and the hottest switch at any mission design point is used to define the inverter required coolant temperature. This required coolant temperature value is used in TMS system design as described in Section G. If this temperature is below 50 C, the design tool redesigns the inverter with added mass per Section D.

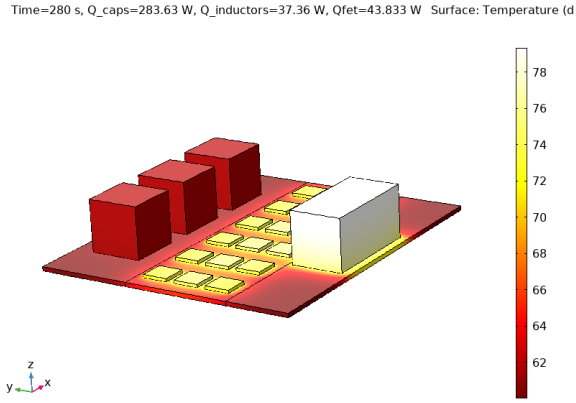

Figure 3 Inverter Thermal Model Example Result

F. Motor Winding Static Thermal and Mechanical Stress Analysis

Similar to the inverter thermal FEA model, a motor winding thermal and mechanical stress model is used to define the max allowable temperature of the motor coolant in cruise and the max allowable temperature for the windings to not exceed the assumed mechanical stress limit. A single half slot of the motor winding is simulated in both cruise and climb conditions. An example simulation geometry and winding thermal and structural results are shown in Figures 4 and 5. The cruise result is used directly to define the max allowable motor

coolant temperature in cruise for initial TMS design as described in Section G. The mechanical stress results in both climb and cruise are used to create a linear interpolation for peak shear stresses in the coil as a function of temperature. Shear stress is used as the metric for coil mechanical failure assuming delamination of insulation layers and epoxy from the copper and stator iron is the likely failure mode.

The motor thermal model is also used to generate a thermal reluctance model of the motor for TMS system design. Effective resistances and thermal inertias of the stator windings, stator back iron, and heat sink are evaluated from the FEA result and the part geometries.

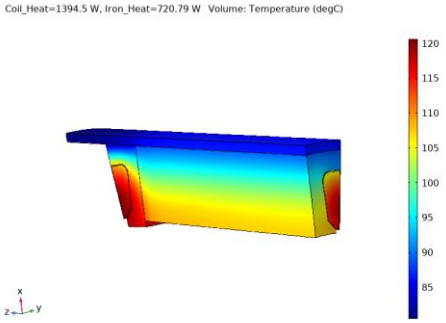

Figure 4 Example Motor Winding Static Thermal Result

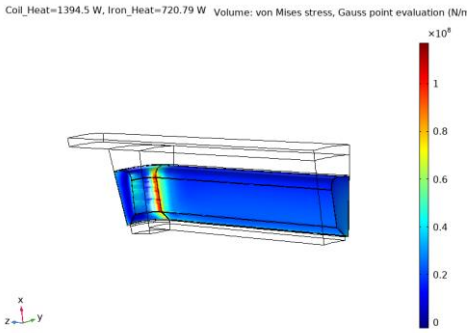

Figure 5 Example Motor Winding Static Mechanical Stress Result in Pa

G. TMS System Design

An iterative solver is used to design a TMS system for the inverter, motor, and gearbox. The required steady state coolant conditions of both the motor and the inverter as well as their losses, and the gearbox losses are used to define the required inlet and outlet condition of the coolant from the thermal management system's air to liquid heat exchangers. HEATSSPY [13] is integrated into the design tool and used to optimize the size and effectiveness of the air to liquid heat exchangers for steady state cruise. Plate-fin surfaces are chosen as the heat exchanger type to minimize weight.

After the air to liquid heat exchanger design is optimized, a thermal reluctance model for the full system (motor, inverter, gearbox, and heat exchanger) is assembled and a transient simulation of the mission profile is run to get estimates of component and coolant temperatures throughout the mission profile. Figure 6 shows an example result from this reluctance model. If a component is predicted to exceed its allowable temperature in the thermal simulation, the TMS design is redone with lower required coolant temperatures either until the design closes or the required coolant temperature drops below 50 C.

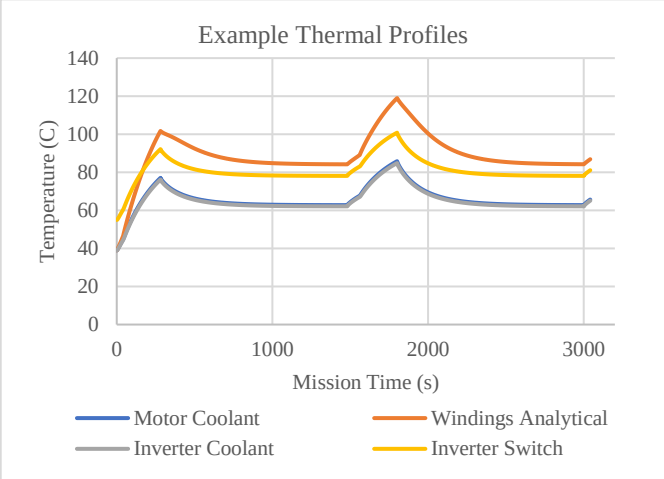

Figure 6 Example Coolant and Component Thermal Transient Results from Simple Reluctance Model

H. Motor Transient Thermal Analysis

As a final thermal analysis of the motor, a 3D transient thermal FEA of the machine is completed using the model described in [1]. The motor coolant temperature vs mission time profile is taken from the reluctance model described in Section G and a full mission profile transient analysis is completed. The absolute peak winding temperature from this analysis is input into the linear fit for winding shear stress Vs temperature from the static model in Section F to estimate peak coil mechanical stresses and eliminate designs that exceed the specified limit. A coil thermal chemical aging life prediction is made based on the assumed thermal class of the insulator [1]. Motors not able to meet a minimum target winding life (10,000 missions in this paper) are eliminated from consideration.

III. QUADROTOR OPTIMIZATION STUDY

For the quadrotor optimization, two runs of the genetic optimization were completed. Each run used a population of 100 designs over 20 generations. The value ranges for the genetic optimization variables used in each run are summarized in Table 4. Roughly 1000 fitness evaluations were completed per run. A total of 1069 valid designs were found. Total mission efficiency and total system mass are plotted for all designs under 70 Kg in Figure 7. The pareto front for the optimization is highlighted. Total mission efficiency is defined as total energy out of the system over total energy into the system for the nominal mission (no engine out).

Table 4 Genetic Optimization Variable Ranges

Variable	Run1	Run2
Pole Pairs	3-10	4-9
Electrical Frequency (kHz)	0.75-2	0.5-1.3
Motor Tip Speed (m/s)	50-200	50-100
Magnet Thickness (mm)	10-20	10-20
Motor Mass (kg)	10-50	13-24
Coolant Flow ($10^{-3}m^3/s$)	0.5-10	0.01-3

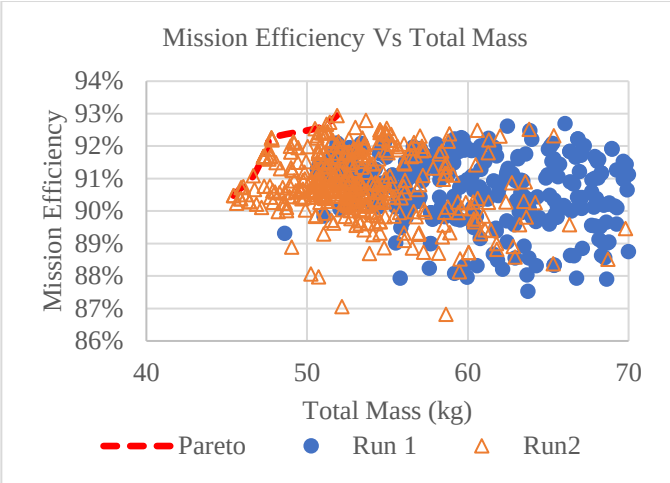

Figure 7 Mission Efficiency Vs Total Mass for All Valid Designs Less than 70 Kg

From Figure 7, along the pareto front, mass ranges from 45.4 to 51.2 kg and total mission efficieny ranges from 90.47% to 92.68%. Four designs from along the pareto front are summarized in Table 5. In the table the highest efficiency design has a higher motor RPM, lower electrical frequncy, and a lower pole count than the lowest mass design. Mass difference between the designs is primarily driven by the motor and gearbox masses. Figures 8 and 9, illustrate the trend of efficiency increasing with decreased electrical frequency and the total mass trend with motor mass.

Table 5 Details of 4 Pareto Front Designs

Design #	**1**	**2**	**3**	**4**
Pole Pairs	9	7	4	5
Electrical Frequency (Hz)	955	802	762	775
Motor RPM	6,367	6,874	11,430	9,300
Tip Speed (m/s)	53	57	67	67
Magnet Thickness (mm)	14	16	19	20
Fluid Coolant Flow ($10^{-3}m^3/s$)	0.35	1.94	0.45	0.48
Switching Frequency (kHz)	70	55	50	50
Switch Count	108	84	96	60
Coil Shear Stress (MPa)	12.8	11.8	11.8	12.9
Thermo-Chemical Life Consumed (%)	44.4%	3.4%	1.0%	2.6%
Peak Winding Temperature (C)	254	212	196	211
Peak Inverter Temperature (C)	136	140	138	133
Peak Inverter Coolant Temperature (C)	73	67	66	65
Peak Motor Coolant Temperature (C)	86	69	74	72
Inverter Mass (kg)	6.27	4.54	3.67	6.96
Motor Mass (kg)	18.12	19.86	20.97	21.45
Gearbox Mass (kg)	18.98	19.19	20.71	20.08
Liquid to Air Hx Mass (kg)	2.07	3.70	2.45	2.71
Total Mass (kg)	45.4	47.3	47.8	51.2
Inverter Mission Efficiency	95.2%	96.3%	96.3%	96.9%
Motor Mission Efficiency	96.4%	96.8%	97.3%	97.2%
Gearbox Efficiency	99.1%	99.1%	99.1%	99.1%
Fluid Pumping Power (W)	5.4	184	13.75	43.7
Mission Efficiency	90.47%	91.68%	92.25%	92.68%

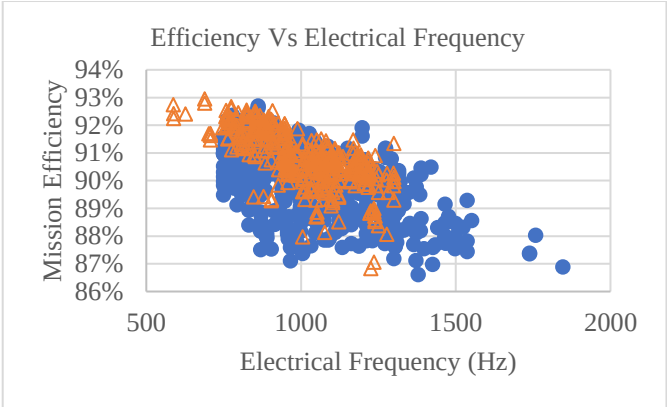

Figure 8 Mission Efficiency Vs Motor Electrical Frequency for all Designs

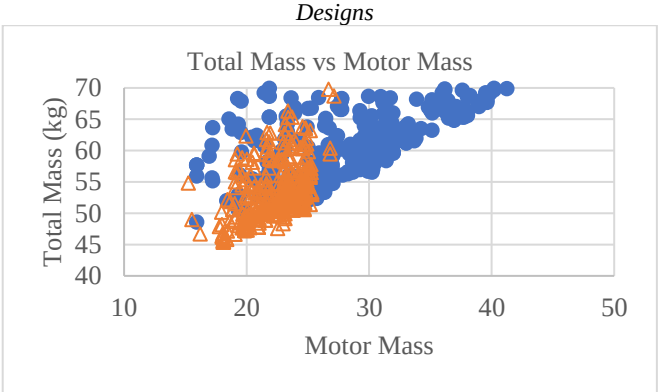

Figure 9 Total Mass Vs Motor Mass

The efficiency trend with electrical frequency is primarily explained by the required switching frequency in the inverter needed to drive higher frequency motors as well as the finding in [1] that speed/frequency dependent losses are the primary overall driver of mission efficiency. The trend is however relative to the assumptions of this paper, constant motor RPM, constant switching frequency, and assumed inverter current ripple requirements.

The mass trend in Figure 9 has close to a one to one ratio of increase in motor mass to increase in total mass. Motor mass is primarily driving the overall mass as the inverter, TMS, and gearbox mass are relatively insensitive to the design variables. The choice to design the inverter for min mass in the design tool likely is the reason for the inverter's low impact on overall mass. If an alternative objective was used for inverter design, the results would likely be different. Gearbox mass variation in the design space can be inferred from Equation 1. TMS system mass trended with the required coolant temperatures in the range of 2 to 8 kg.

Typically, motor mass is known to scale with torque. Correspondingly one would expect that the lowest mass drive would have the fastest motor. However, the lightest weight design in Table 5 has the lowest RPM. This counter-intuitive trend relates to the shear stress limit put on the motor designs and its relation to stator coil width and correspondingly motor pole count.

Figure 10 shows peak winding temperature vs motor mass. The expected trend of a lighter motor running hotter is shown. It is, however, worth noting that even the lightest motor only consumed 44% of its thermal chemical aging life and

correspondingly absolute temperature did not limit the specific power in any of the valid designs. Figure 11 shows coil shear stress vs motor mass. Results shows that a number of designs did reach the shear stress limit of 13 MPa applied in this paper and correspondingly, shear stress was limiting for motor specific power in the design space.

Motor shear stress per degree stator coil temperature vs motor coil width is shown in Figure 12. The trend of smaller width coils leading to less stress per motor temperature is shown. The overall result is that higher pole count motors with lower RPM are able to weigh less than lower pole count motors with higher RPM because they can operate at higher temperatures with less shear stress. Both stronger materials and better coil design would change this trend and enable higher motor specific power.

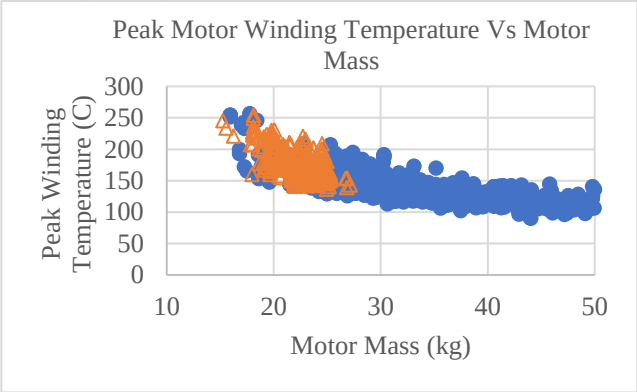

Figure 10 Motor Peak Winding Temperature Vs Motor Mass

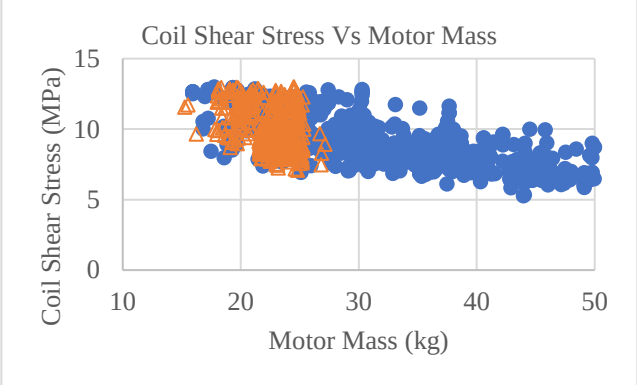

Figure 11 Motor Coil Shear Stress Vs Motor Mass

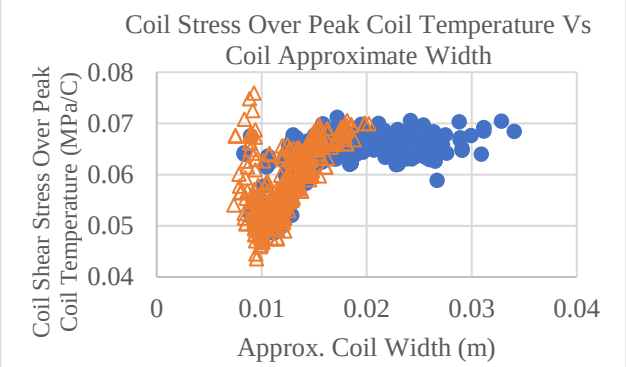

Figure 12 Coil Stress Over Peak Temperature Vs Coil Width

IV. CONCLUSION

In this paper, a first version of an electric motor drivetrain tool for electric aircraft drivetrains was presented. Preliminary results for the NASA RVLT 6 passenger quad rotor concept vehicle were presented. Design trends show that motor electrical frequency was a primary driver for overall drive efficiency, while motor mass (constrained primarily by motor coil shear stress) was the driver of overall drivetrain mass. Near term future work on the design tool will focus on increasing the speed of the optimization.

V. REFERENCES

[1] T. F. Tallerico, "NASA Reference Motor Designs for Electric Vertical Takeoff and Landing Vehicles," in *AIAA Propulsion and Energy 2021 Forum*, Virtual, 2021.

[2] C. Silva, W. Johnson, K. Antcliff and P. D. Michael, "VTOL Urban Air Mobility Concept Vehicles for Technology Development," in *AIAA Aviation*, Alanta, 2018.

[3] M. Garrett, D. Avanesian, M. Granger, S. Kowalewski, J. Maroli, W. Miller, R. Jansen and P. Kascak, "Development of an 11 kW lightweight, high efficiency motor controller for NASA X-57 Distributed Electric Propulsion using SiC MOSFET Switches," in *AIAA Propulsion and Energy 2019 Forum*, Indianapolis, 2019.

[4] A. Leary, V. Keylin, R. Noebe, R. Bowman, G. Feichter, K. Byerly, P. Ohodnicki and M. Mchenry, "Core Losses in Co-rich Inductors with Tunable Permeability," in *TMC*, 2020.

[5] C. Silva, W. Johnson, K. Antcliff and P. D. Michael, "VTOL Urban Air Mobility Concept Vehicles for Technology Development," in *AIAA Aviation*, Alanta, 2018.

[6] T. F. Tallerico, "Genetic Optimization of Planetary Gearboxes Based on Analytical Gearing Equations," NASA, Cleveland, 2022.

[7] Z. P. Xia, Z. Q. Zhu and D. Howe, "Analytical Magnetic Field Analysis of Halbach Magnetized Permanent-Magnet Machines," *IEEE TRANSACTIONS ON MAGNETICS*, vol. 40, no. 4, 2004.

[8] L. Chang, "An Improved FE Inductance Calculation for Electrical Machines," *IEEE 1RANSACTIONS ON MAGNETICS,*, vol. 32, no. 4, pp. 3237-3245, 1996.

[9] D. Graovac, M. Purschel and K. Andreas, "MOSFET Power Losses Calculation Using the Data-Sheet Parameters," July 2006. [Online]. Available: https://www.digchip.com/application-notes/48/41484.php. [Accessed December 2021].

[10] G. Grandi and J. Loncarrski, "Evaluation of Current Ripple Amplitude in Three-Phase PWM Voltage Source Inverters," in *International Conference-Workshop Compatibility And Power Electronics*, 2013.

[11] J. W. Jolar, T. M. Wolbank and M. Schrodl, "Analytical calculation of the RMS current stress on the DC link capacitor of voltage DC link PWM converter systems," in *Ninth International Conference on Electrical Machines and Drives*, 1999.

[12] E. Levi, D. Dujoc, M. Jones and G. Grandi, "Analytical Determination of DC-Bus Utilization Limits in Multiphase VSI Supplied AC Drives," *IEEE TRANSACTIONS ON ENERGY CONVERSION*, vol. 2, no. 2, pp. 466-443, 2008.

[13] J. Chapman, H. Hasseeb and S. Schnulo, "Thermal Management System Design for Electrified Aircraft Propulsion Concepts," in *AIAA Propulsion and Energy 2020 Forum*, Virtual, 2020.

[14] T. Cao and A. P. Thurlbeck, "Heavy-duty UAV Electrical Propulsion Architectures and Multi-timescale Multi-physics Modeling," in *AIAA Propulsion and Energy Forum*, Indianapolis, 2019.